Near-surface water vapor over polar sea ice is always near ice saturation

Edgar L Andreas
U.S. Army Cold Regions Research and Engineering Laboratory, Hanover, New Hampshire, USA

Peter S. Guest
Department of Meteorology, Naval Postgraduate School, Monterey, California, USA

P. Ola G. Persson
Cooperative Institute for Research in Environmental Sciences, University of Colorado, Boulder, Colorado, USA

Christopher W. Fairall
NOAA Environmental Technology Laboratory, Boulder, Colorado, USA

Thomas W. Horst
National Center for Atmospheric Research, Boulder, Colorado, USA

Richard E. Moritz
Polar Science Center, University of Washington, Seattle, Washington, USA

Steven R. Semmer
National Center for Atmospheric Research, Boulder, Colorado, USA

Received 2 May 2000; revised 22 January 2001; accepted 12 September 2001; published 30 August 2002.

[1] During our yearlong participation in the Surface Heat Budget of the Arctic Ocean experiment (SHEBA), we found the measured relative humidity, figured for saturation with respect to ice, to almost always be near 100%. Often, multiple humidity sensors even showed supersaturation. Four months of observations over sea ice in the Antarctic showed the same behavior. These frequent, ubiquitous, and reproducible measurements are too compelling to discount. We hypothesize that the high relative humidity is a consequence of plentiful water vapor given up by leads and polynyas. We thus develop a simple time-dependent vapor budget model that we solve analytically to assess the role of leads in supplying water vapor to the polar atmospheric boundary layer. The solution to that model shows that (1) because the polar marine boundary layer is generally thin, its timescale for reaching moisture equilibrium is much shorter than the timescale of the synoptic processes that tend to disrupt equilibrium, and (2) because they have relatively warm surfaces, open leads and polynyas supply water vapor more rapidly than the surrounding sea ice surface can remove it, despite an open water fractional area that may be only 5%. In concert, the two processes commonly lead to water vapor densities in the boundary layer over sea ice that are near the value for ice saturation. *INDEX TERMS:* 3307 Meteorology and Atmospheric Dynamics: Boundary layer processes; 3349 Meteorology and Atmospheric Dynamics: Polar Meteorology; 3394 Meteorology and Atmospheric Dynamics: Instruments and techniques; 4540 Oceanography: Physical: Ice mechanics and air/sea/ice exchange processes; *KEYWORDS:* air-sea-ice interaction, humidity measurements, leads, polar marine boundary layer, SHEBA, water vapor

1. Introduction

[2] During our yearlong deployment for the Surface Heat Budget of the Arctic Ocean experiment (SHEBA), we frequently experienced fog, rains of "diamond dust," and episodes of severe hoarfrost and rime that accumulated on any and all structures. These casual observations suggest that the near-surface relative humidity is often near ice saturation over Arctic sea ice.

[3] Besides these qualitative observations, however, we had the most extensive array of humidity sensors ever assembled on sea ice—more than a dozen instruments spread

Copyright 2002 by the American Geophysical Union.
0148-0227/02/2000JC000411$09.00

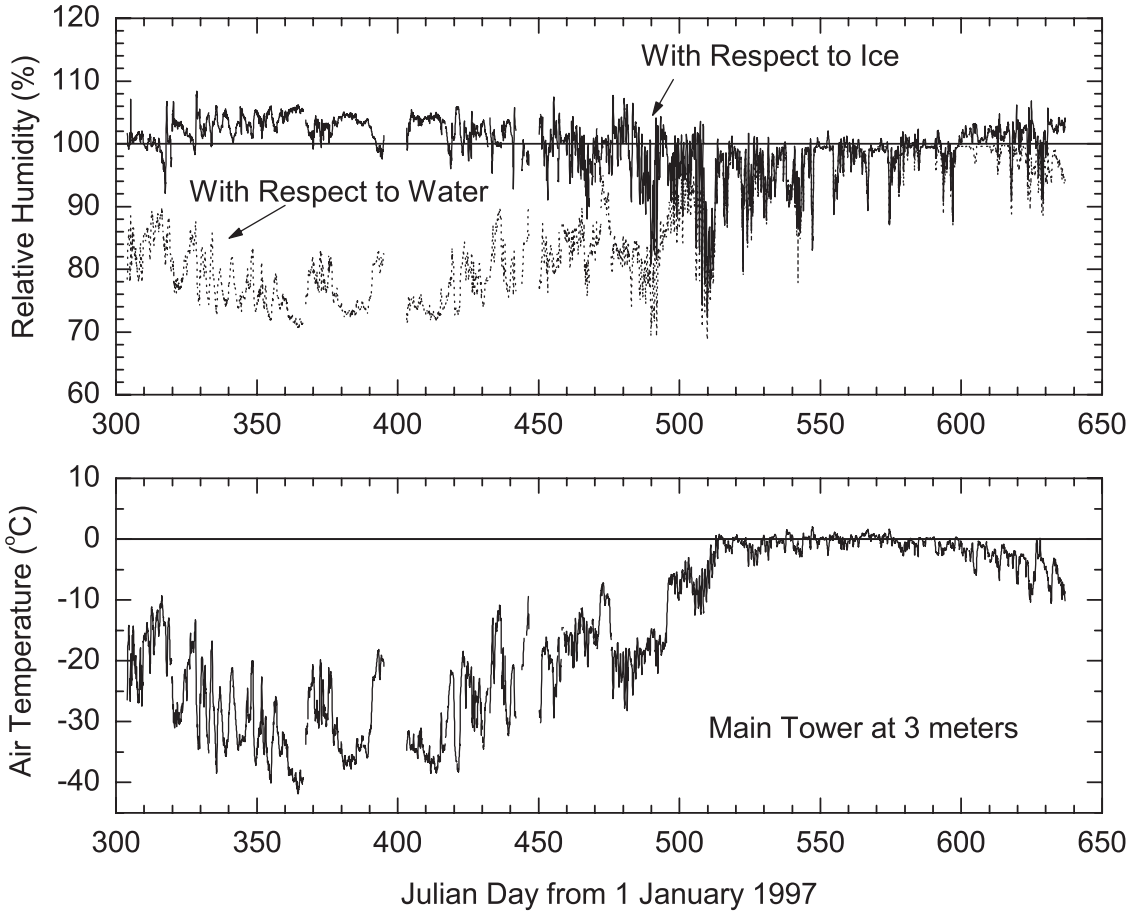

Figure 1. Hourly averaged values of the temperature and the relative humidities with respect to both water and ice for the duration of our SHEBA deployment, as measured at the 3-m level on our main tower.

among several sites. All of these agreed that the near-surface relative humidity, figured with respect to ice saturation, is very near 100% year-round. Another humidity sensor that operated for four months in 1992 on Ice Station Weddell confirmed the same observation over Antarctic sea ice.

[4] *Sverdrup* [1933, p. 250 ff.] reported the same result over 60 years ago based on 150 observations during the Norwegian North Polar Expedition on the *Maud*. Data collected during the 1893–1896 drift of the *Fram*, though less reliable, also suggest relative humidities above 90% with respect to ice in all seasons [*Persson et al.*, 2002]. Likewise, *Vowinckel and Orvig* [1970, p. 206 ff.] argued that, in winter in the Arctic Basin, the relative humidity with respect to ice should be 100% or better; while the *Treshnikov* [1985, p. 78] atlas shows one climatological plot for January with the surface-level relative humidity over the entire Arctic Ocean at or above ice saturation.

[5] Because of the difficulty in measuring humidity at low temperature and the consequent absence of a definitive polar climatology, not all have recognized this prevalence of near-saturation. For example, although he based his choices on the best data available at the time, *Maykut* [1978] assumed that the monthly mean relative humidity with respect to ice saturation in the central Arctic in the winter was 90% and in other months was between 91 and 96%. On analyzing 45 station-years of data from the Russian North Pole (NP) drifting stations, *Lindsay* [1998] produced monthly averaged values of relative humidity with respect to water. On converting these to relative humidity with respect to ice, we see that his winter means correspond to values well above ice saturation, while his summer means correspond to values significantly below ice saturation. Finally, after analyzing radiosounding data from the NP stations, *Curry et al.* [1995] concluded that, from 15 September through 1 May, the relative humidity in the layer between the surface and 850 mb over the Arctic Ocean is about 93% with respect to ice saturation. They speculated that falls of ice crystals constrain the relative humidity to ice saturation or below.

[6] Here we treat this question of the relative humidity over sea ice. We show with multiple SHEBA humidity sensors that, although the relative humidity with respect to water and the variability in the relative humidity with respect to ice have annual cycles, the mean value of the relative humidity with respect to ice has very small month-to-month variability. We also develop a simple atmospheric boundary layer model to explain why the relative humidity over perennial sea ice is near ice saturation. This model also helps us understand why the relative humidity over another saturated surface, the open ocean, is typically well below saturation. Finally, we identify apparent measurement errors in our humidity sensors at temperatures below −25°C and discuss how these affect our conclusions.

[7] The main objectives of SHEBA are to develop better parameterizations for the surface heat budget of an ice-covered ocean and to better understand the feedback among

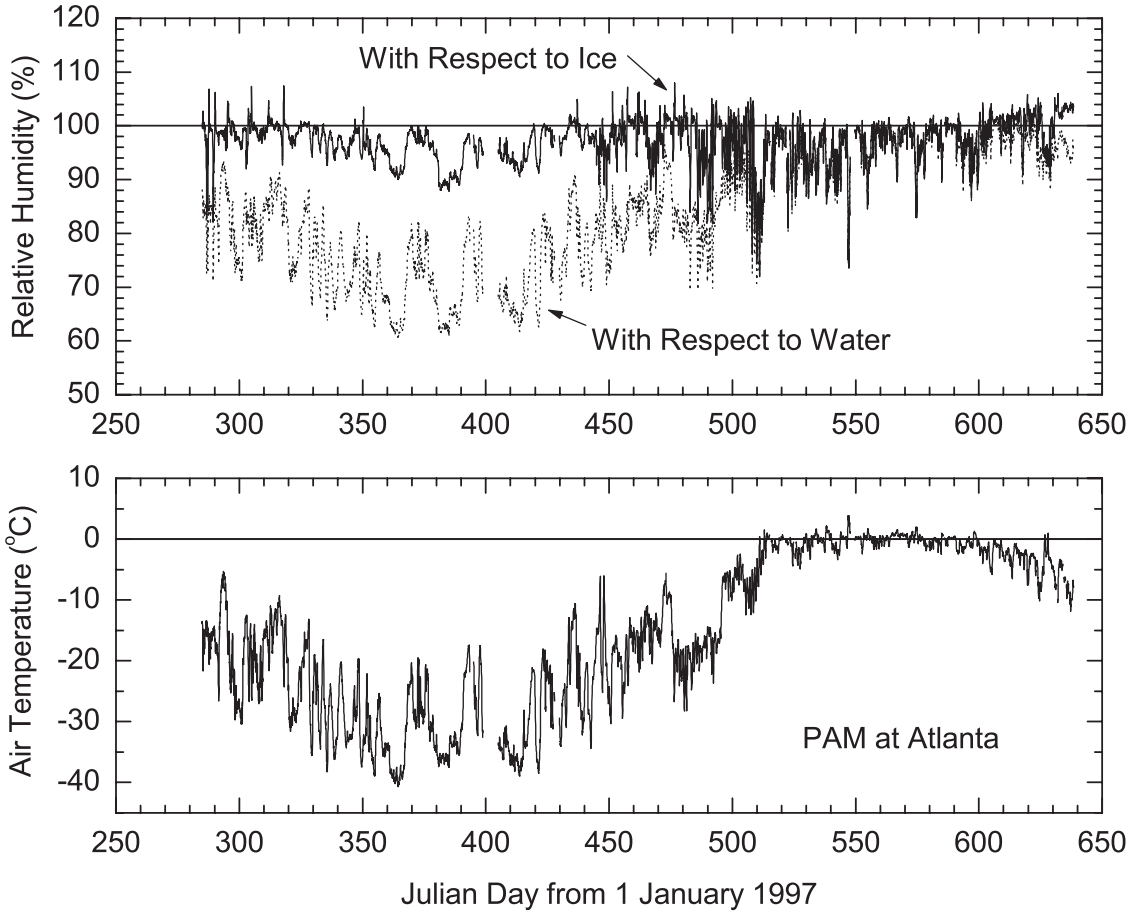

Figure 2. As in Figure 1, except these data come from the PAM station at Atlanta, which was about 1 km from the main camp.

clouds, radiation, and surface albedo. The humidity of the atmospheric boundary layer is rolled up in all of these processes. It is part of the driving term that dictates the turbulent surface flux of latent heat, which is a component of the surface heat budget. Likewise, the relative humidity in the boundary layer influences the abundance and size distribution of the droplets in low-level clouds that, in turn, control the components of both the longwave and shortwave radiation at the surface. Our finding that the near-surface relative humidity over perennial sea ice is near ice saturation year-round could, thus, reduce observational demands and may let modelers simplify some of the parameterizations required to compute the surface heat budget.

2. Observations

[8] SHEBA is an international, multidisciplinary program of research into the processes that influence the surface heat budget of the Arctic Ocean [*Moritz et al.*, 1993; *Moritz and Perovich*, 1996]. Its experimental center was the Canadian Coast Guard icebreaker *Des Groseilliers*, which spent 2 October 1997 to 11 October 1998 frozen into sea ice and drifting from the Beaufort to the Chukchi Sea and then into the Arctic Ocean [*Perovich et al.*, 1999].

[9] The main emphasis of the SHEBA Atmospheric Surface Flux Group (ASFG) was to measure all the components of the surface heat budget at the main camp and at several remote locations [*Andreas et al.*, 1999; *Persson et al.*, 2002]. To develop parameterizations for these fluxes, however, we also measured mean meteorological quantities, such as wind speed, temperature, and relative humidity, at the same sites. Many of our instruments in the main camp were mounted on a 20-m tower about 300 m from the *Des Groseilliers*. This tower had five levels of identical instruments at nominal heights of 2, 3, 5, 9, and 18 m. The temperature and humidity sensors on this tower were Vaisala model HMP235's. For measuring humidity, these use Vaisala's popular Humicap, which is a capacitance sensor that reports the relative humidity with respect to saturation over water. Both the temperature and humidity sensors were mounted on the tower in aspirated radiation shields.

[10] The ASFG also maintained four remote sites ranging in distance between 0.4 and 10 km from the *Des Groseilliers*. We identified these four remote sites as Atlanta, Baltimore, Cleveland, and Florida—the teams that were playing in the Major League Baseball Championship Series while we were building the SHEBA camp in the fall of 1997. Each site was instrumented with a portable automated mesonet (PAM) station designed and built at the National Center for Atmospheric Research as a principal component of the NCAR Integrated Surface Flux Facility. These were Flux-PAM stations that measured all the quantities we measured on and around the main tower [*Militzer et al.*,

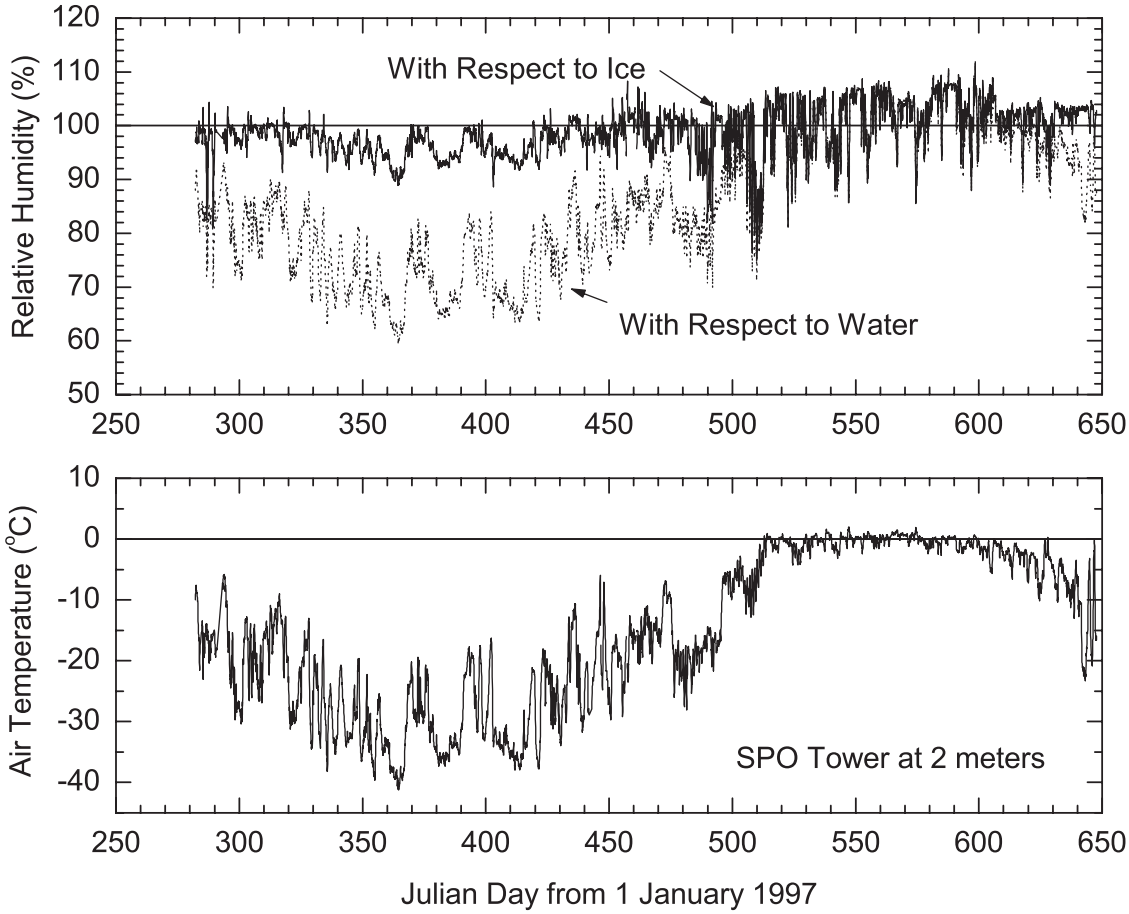

Figure 3. As in Figure 1, except these data come from the 2-m level of the best exposed of the two towers maintained by the SHEBA Project Office.

1995] but at one level only, typically 1.8 m for the relative humidity and temperature. The humidity sensors on the Flux-PAM stations were also Vaisala probes, the model HMD50Y. These use the Intercap, an interchangeable capacitance element, as their humidity sensor. As on the main tower, these temperature and humidity sensors were in an aspirated radiation shield.

[11] The SHEBA Project Office (SPO) maintained two 10-m towers in the main SHEBA camp to provide routine meteorological data. One was on the sea ice to the port side of the *Des Groseilliers*; the other was on ice on the starboard side. Each tower had Vaisala HMD50U relative humidity sensors at 2 and 10 m; the sensing element in each of these was also the Intercap. Again, each sensor was in an aspirated radiation shield. The values reported in the SPO data set are from the tower with the best exposure to undisturbed conditions.

[12] The humidity sensors on the PAM stations were calibrated before the SHEBA experiment at −15°C in the NCAR Sensor Calibration Laboratory, and all the SHEBA humidity sensors we use here were calibrated after the experiment in the same facility. Briefly, these calibrations showed that our sensors were accurate to within about 2–4% in relative humidity for humidities typical of the SHEBA environment. More specifically, the ASFG tower humidity sensors tended to read low by 1–5%, the PAM sensors tended to read low by 2–4%, and the SPO sensors fell into two groups. SPO sensors used up to SHEBA day 610 tended to read high during the post-experiment calibration by 1–4%, while replacement sensors installed on about day 610 tended to read low by 1–3%. Web sites at http://www.met.nps.navy.mil/~guestps/sheba/ and http://www.atd.ucar.edu/sssf/projects/sheba/ provide more information on our SHEBA instruments and these calibrations.

[13] Figures 1–3 show hourly averaged values of temperature and relative humidity from a representative sample of these 13 humidity sensors. As we mentioned, the fundamental humidity variable that each instrument reported was the relative humidity with respect to water (RH_w). That series is the dotted line in each plot. We converted this value to the relative humidity with respect to ice saturation (RH_i) using

$$RH_i = RH_w \left[\frac{e_{sat,w}(T_a)}{e_{sat,i}(T_a)}\right], \tag{2.1}$$

where for $-40°C \leq T_a \leq 0°C$ [*Buck*, 1981]

$$e_{sat,w}(T_a) = \left(1.0007 + 3.46 \times 10^{-6}\ P\right) 6.1121 \exp\left(\frac{17.966 T_a}{247.15 + T_a}\right), \tag{2.2}$$

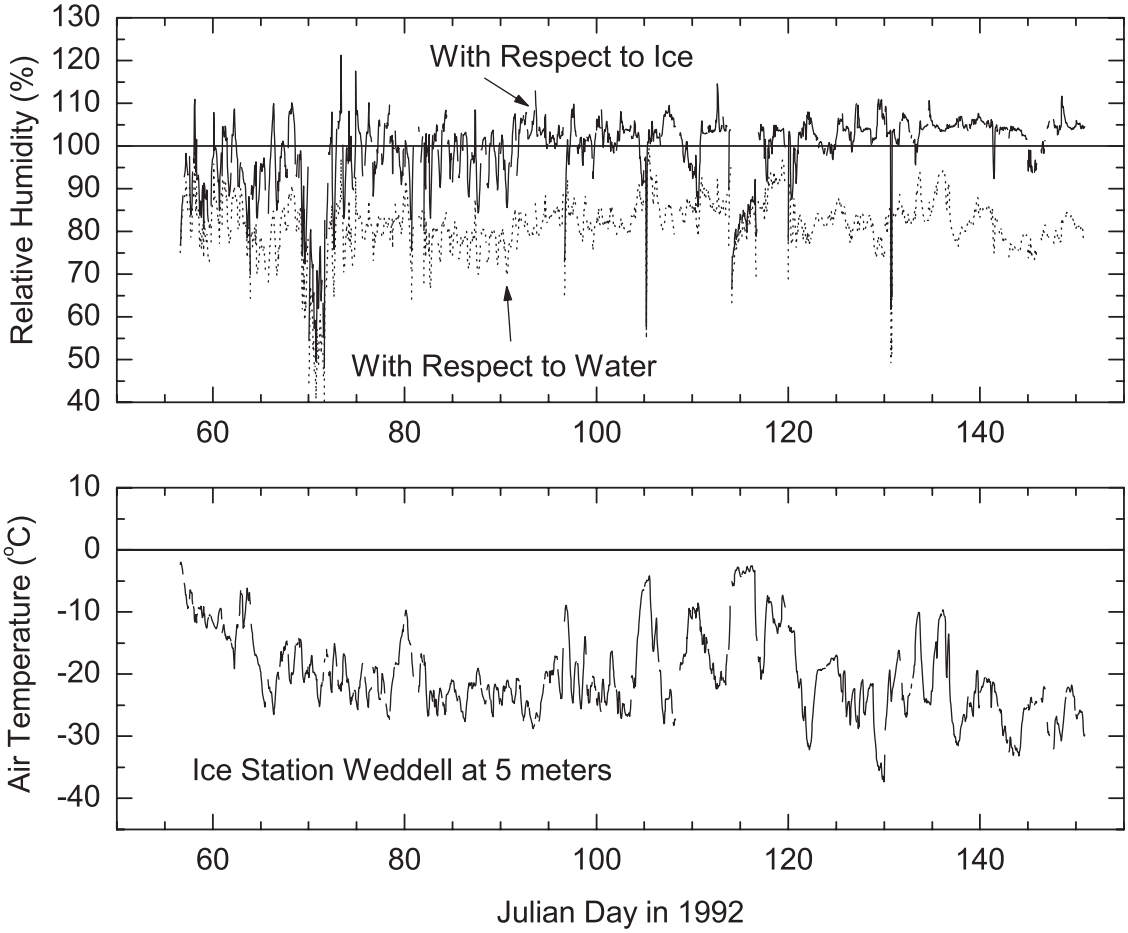

Figure 4. As in Figure 1, except these data come from a platinum resistance thermometer and a cooled-mirror dew-point hygrometer operated for almost four months on Ice Station Weddell in the Antarctic.

and for $-50°C \leq T_a \leq 0°C$

$$e_{sat,i}(T_a) = \left(1.0003 + 4.18 \times 10^{-6}\ P\right)6.1115\exp\left(\frac{22.452T_a}{272.55 + T_a}\right). \tag{2.3}$$

Here T_a is the measured air temperature in degrees Celsius, P is the barometric pressure in millibars, and the saturation vapor pressures over water and ice, $e_{sat,w}$ and $e_{sat,i}$, respectively, are in millibars. That RH_i series is the solid line in the upper panel of each plot.

[14] In each plot, the air temperature reaches a minimum near −40°C around 1 January 1998. The relative humidity with respect to water is at or near its minimum value of 60–70% at approximately this same time. From there it begins a gradual climb toward its summertime level of 100%. The relative humidity with respect to ice, on the other hand, shows little seasonal change in its mean; it hangs around 100% throughout the year. Its variability is much less in winter than in summer, though.

[15] All the other SHEBA humidity sensors show this same behavior: RH_w ranges from values as low as 60–70% in winter to 100% in summer, while RH_i has a mean that is within a few percent of 100% year-round.

[16] During the four-month drift of Ice Station Weddell (ISW) in the western Weddell Sea in the austral fall of 1992 [*ISW Group*, 1993; *Andreas and Claffey*, 1995], we made additional humidity measurements over sea ice. For these, we used a General Eastern 1200MPS cooled-mirror dew-point hygrometer mounted 5 m above the sea ice surface. In this instrument, platinum resistance thermometers are used to sense both the air temperature and the temperature of the mirror. Again, both sensors were in an aspirated radiation shield. Figure 4 shows values of air temperature, RH_w, and RH_i obtained with this instrument. This Antarctic record is not as long, but we see the same trends we find during SHEBA: In the fall, RH_w is about 80%, while RH_i is near 100% on average.

[17] Table 1 summarizes the monthly averages of air temperature, surface temperature, RH_i, and the standard deviation of RH_i for the data depicted in Figures 1–4. We can use a Student's t-statistic to calculate a 99% confidence interval for the monthly mean relative humidities. Since each monthly mean derives from about 700 observations, the 99% confidence interval for the mean ($\overline{RH_i}$) is, in general, approximately $\overline{RH_i} \pm 0.1s$, where s is the tabulated sample standard deviation. Because we have so many observations each month, the 99% confidence interval about $\overline{RH_i}$ is fairly small, typically ±0.3% for the

Table 1. Monthly Averaged Values of Temperature and Relative Humidity With Respect to Ice From SHEBA and From Ice Station Weddell[a]

	SHEBA											Ice Station Weddell			
			Main Tower, 3 m			PAM at Atlanta			SPO Tower, 2 m						
	T_a, °C	T_i, °C	No.	RH_i, %	S.D., %	No.	RH_i, %	S.D., %	No.	RH_i, %	S.D., %	No.	T_a, °C	RH_i, %	S.D., %
Oct	−16.45					481	98.28	3.06	665	99.29	3.32				
Nov	−21.14	−21.53	739	101.24	2.19	720	99.10	1.71	708	98.60	1.66				
Dec	−32.57	−34.13	744	103.86	1.38	744	95.48	2.46	743	94.80	2.39				
Jan	−29.72	−30.30	666	102.65	1.73	709	94.43	3.70	744	96.01	2.46				
Feb	−32.00	−33.06	509	102.90	1.99	524	95.21	2.61	659	95.44	2.32	94	−9.55	91.36	6.66
Mar	−22.78	−23.10	552	100.93	2.27	690	97.92	2.57	719	98.70	2.00	658	−20.11	95.15	10.24
Apr	−17.17	−17.35	682	99.39	3.28	719	99.01	3.60	686	99.68	2.70	663	−17.36	99.80	7.53
May	−9.26	−8.90	742	94.20	6.34	729	94.64	6.48	742	96.26	6.54	633	−23.98	103.56	3.89
Jun	−0.77	−0.66	711	95.45	3.60	675	95.02	4.21	720	99.88	5.06				
Jul	0.06	−0.18	723	97.91	2.96	700	96.58	4.24	744	102.33	4.49				
Aug	−1.20	−1.17	722	99.75	1.90	716	98.35	2.91	744	103.78	3.58				
Sep	−4.33	−4.01	666	101.33	2.33	661	100.43	2.95	720	101.09	2.58				

[a] T_a is the air temperature, T_i is the surface temperature of the sea ice, No. is the number of hourly averaged values used in computing the relative humidity statistics, RH_i is the relative humidity with respect to ice, and S.D. is the standard deviation of RH_i. For the SHEBA set, T_a was measured on the main tower at 3 m in all months except October, when it comes from the 2-m level of the SPO tower.

SHEBA data and somewhat larger for the ISW data. Thus, although 100% is not always within the 99% confidence interval for each monthly mean, the data do suggest that the relative humidity with respect to ice is above 95% in all seasons.

[18] Table 1 has one curious feature. For the coldest months of SHEBA, December, January, and February, the relative humidity measured at the main tower is significantly above 100%, while humidities measured at the PAM stations and on the SPO towers are significantly below 100%. In most other months, the three sensors are quite compatible. Later, we will ascribe this difference in humidities during the coldest months to differences in the behaviors of the sensors on the main tower and on the PAM stations and on the SPO towers.

3. A Simple Water Vapor Model

[19] The data shown in the last section and all the other SHEBA humidity data that we have not shown make the same point: Near-surface water vapor over polar sea ice is always near its saturation value with respect to ice. Admittedly, the water vapor in immediate contact with a snow or sea ice surface is in equilibrium with respect to ice saturation [e.g., *Andreas*, 1986; *Andreas and Cash*, 1996]. But why does vapor a few meters above the surface still have a density defined by ice saturation? After all, the near-surface relative humidity over the ocean—another extensive saturated surface—is not always 100% with respect to water saturation [e.g., *Hsiung*, 1986]. Something seems fundamentally different about moisture processes in the polar marine atmospheric boundary layer (ABL).

[20] We hypothesize that open leads and polynyas explain the near saturation over Arctic and Antarctic sea ice. Leads and polynyas are areas of open water surrounded by insulating ice. In a nutshell, they expose relatively warm ocean water to the cold atmosphere. This warm water gives up water vapor to the atmosphere much more rapidly than does the colder surface of the surrounding sea ice. In other words, leads and polynyas could conceivably supply so much vapor that, when spread over the ice-covered areas, this vapor would be far in excess of what could be in equilibrium with the sea ice.

[21] *Anderson*'s [1993] observations at Halley Station, on the Brunt Ice Shelf, Antarctica, support this hypothesis. He found good correlation between episodes of fog under westerly wind at Halley with the occurrence of a coastal polynya in the Weddell Sea a few tens of kilometers upwind. We, therefore, develop a very simple model of the moisture content of the ABL over sea ice that demonstrates how only a few percent open water can supply enough moisture to bring the ABL to ice saturation and beyond in just a few hours because of the relative rapidity of this moisture exchange from open leads and polynyas.

[22] Both sea ice and the surface water in leads and polynyas exchange water vapor with the atmosphere. We model those water vapor fluxes over leads and over sea ice, E_w and E_i, respectively, as

$$E_w = U_{10}\, C_{E10w}\, (\rho_{vw} - \rho_{v10}), \tag{3.1}$$

$$E_i = U_{10}\, C_{E10i}\, (\rho_{vi} - \rho_{v10}). \tag{3.2}$$

Here, C_{E10w} and C_{E10i} are the bulk transfer coefficients for water vapor over open leads and over sea ice appropriate at a reference height of 10 m, ρ_{vw} is the density of water vapor in saturation with a water surface with temperature T_w, and ρ_{vi} is the water vapor density in saturation with sea ice with surface temperature T_i. Finally, we assume the leads are small enough not to create any mesoscale flow; as a result, we can assume the wind speed and water vapor density at 10 m, U_{10} and ρ_{v10}, to be the same over the sea ice and the leads.

[23] For the sake of simplicity, we also assume that $C_{E10w} = C_{E10i} \equiv C_{E10}$. For the neutral-stability transfer coefficients, this is a fairly good assumption; that is, compare the values for each reported by *Andreas and Murphy* [1986] and *Andreas* [1987]. C_{E10w} and C_{E10i} denote stability-corrected values, however. Since the air over leads can be quite unstable, the stability correction for C_{E10w}, especially, could

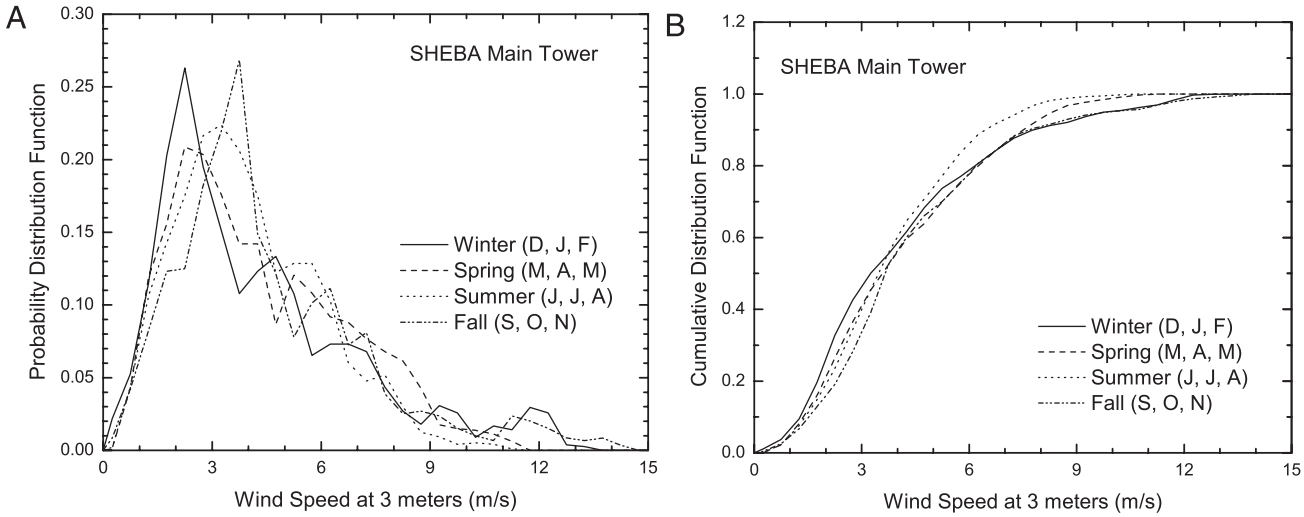

Figure 5. Seasonal distributions of the wind speed measured at 3 m on the main SHEBA 20-m tower. The left panel shows the distribution of speeds in 0.5-m/s bins, while the right panel shows the cumulative distribution.

make it significantly larger than the neutral-stability value C_{EN10w}. Likewise, the stable stratification typical over compact sea ice could significantly reduce C_{E10i} compared to its neutral-stability value C_{EN10i}. We show in the Appendix A, however, that, even if C_{E10w} is a factor of two larger than C_{E10i}, this difference only enhances our essential results.

[24] Consider a polar ABL of height h over a surface comprising open leads of fractional area α and sea ice of fractional area $1 - \alpha$. Both surfaces are exchanging water vapor with the atmosphere at rates given by equations (3.1) and (3.2). If the vapor within the boundary layer is well mixed and has density ρ_{v10}, and if we ignore advection and vapor exchange through the top of the boundary layer, ρ_{v10} evolves with time t according to

$$h\frac{d\rho_{v10}}{dt} = U_{10}\ C_{E10}[(1-\alpha)(\rho_{vi} - \rho_{v10}) + \alpha(\rho_{vw} - \rho_{v10})]. \quad (3.3)$$

Andreas and Makshtas [1985] and *Andreas* [1988] previously used the mosaic technique [e.g., *Vihma*, 1995], represented by the right side of equation (3.3), to compute area-averaged fluxes over sea ice.

[25] Notice that the second term in brackets in equation (3.3) is almost always a source of water vapor since ρ_{vw} is generally much larger than ρ_{v10}. The exception may be in the summer, when the polar marine ABL can be slightly above freezing. The first term in brackets, on the other hand, can be either a source or a sink for water vapor, depending on the sign of $\rho_{vi} - \rho_{v10}$.

[26] For clarity, we rewrite equation (3.3) as

$$\frac{d\rho_{v10}}{dt} = \frac{1}{\tau}\{[(1-\alpha)\rho_{vi} + \alpha\rho_{vw}] - \rho_{v10}\}, \quad (3.4)$$

where

$$\tau = \frac{h}{U_{10}\ C_{E10}}, \quad (3.5)$$

which has units of time.

[27] Without losing any generality, we can assume as a boundary condition that $\rho_{v10} = 0$ at $t = 0$. The solution to equation (3.4) is, thus,

$$\rho_{v10}(t) = [(1-\alpha)\rho_{vi} + \alpha\rho_{vw}][1 - \exp(-t/\tau)], \quad (3.6)$$

or

$$\rho_{v10}(t) = \rho_{vi}\left[1 + \alpha\left(\frac{\rho_{vw}}{\rho_{vi}} - 1\right)\right][1 - \exp(-t/\tau)]. \quad (3.7)$$

4. Model Implications

4.1. Over Sea Ice

[28] Equation (3.7) shows that, in our simple model, the timescale $\tau = h/(U_{10}C_{E10})$ governs the rate at which the polar ABL comes to equilibrium with the surface. With stability corrections included, C_{E10} could range between 1.0×10^{-3} and 2.0×10^{-3} [e.g., *Andreas and Murphy*, 1986; *Andreas*, 1987].

[29] Figure 5 shows the distribution of the wind speed at 3 m (U_3) that we measured with a sonic anemometer on the main 20-m tower during SHEBA. The mode wind speed was between 2 and 4 m/s in all seasons, and U_3 was less than 8 m/s 90% of the time.

[30] From observations with a tethered radiosonde, using the critical Richardson number as a criterion, *Andreas et al.* [2000; see also *Andreas*, 1998] found the height of the ABL over Antarctic sea ice during the ISW observations to be 20–400 m in the fall. Analyses by *Kahl* [1990] and *Serreze et al.* [1992] of archived radiosounding data from in and around the Arctic Basin suggest that the top of the atmospheric inversion, z_i, over the Arctic Ocean might be as high as 800 m in some seasons. Although z_i is often used as an indicator of the top of the ABL and thus as a surrogate for h, for a stable boundary layer, this is not always a valid practice. In a stable ABL, the h in our model equation (3.3) refers to the near-surface atmospheric region that is at least intermittently turbulent [*Mahrt*, 1981; *Zilitinkevich and Mironov*, 1996]. From their Antarctic observations,

Andreas et al. [2000] found that h is typically half of z_i. *Skony et al.* [1994], *Walden et al.* [1996], and *Mahesh et al.* [1997] also suggested that, because of constraints like sensor response, ascent rate, and available technology, older radiosonde systems may not have had the resolution to measure z_i accurately. *Claffey et al.* [1994] documented similar results when they compared measurements from the ISW tethered radiosonde and a free-flying Vaisala Micro-CORA radiosonde. The upshot is that the Arctic inversion heights reported by Kahl and Serreze et al. likely are at least a factor of two larger than h.

[31] Finally, for the stable ABL common over sea ice surfaces, h and U_{10} are correlated, with smaller h associated with lower wind speeds, and larger h associated with higher wind speeds [e.g., *Zilitinkevich and Mironov*, 1996]. Thus, during SHEBA, the ratio h/U_{10} was likely between 10 and 50 s.

[32] Consequently, the probable range of τ is 2–13 hours. That is, the vapor density within the ABL responds fairly quickly to surface conditions. In particular, τ is comparable with or shorter than the time required for a newly opened winter lead to freeze over enough to significantly curtail its flux of water vapor [e.g., *Makshtas*, 1991, p. 26 ff. and Figure 20; *Gow et al.*, 1990; *Wettlaufer et al.*, 2000]. Because Arctic ABL quantities frequently show very little diurnal signal, τ is also much shorter than the only other relevant Arctic timescale: the duration of synoptic systems, which is typically four days.

[33] Given enough time—about 3τ is sufficient—the 10-m vapor density predicted by equation (3.7) will reach the asymptotic limit

$$\rho_{v10,\mathrm{lim}} = \rho_{vi}\left[1 + \alpha\left(\frac{\rho_{vw}}{\rho_{vi}} - 1\right)\right]. \tag{4.1}$$

If T_i and T_{10}, the air temperature at 10 m, are the same, $\rho_{v10,\mathrm{lim}}/\rho_{vi}$ represents the relative humidity at 10 m figured with respect to saturation over ice. Hence, even without leads (that is, if $\alpha = 0$), $\rho_{v10,\mathrm{lim}}/\rho_{vi} = 1$. In other words, without leads, $\rho_{v10,\mathrm{lim}}$ differs from the ice saturation value only if T_i and T_{10} differ. They could differ by a couple of degrees in very stable stratification. But because large differences are rare (see Table 1), and since the timescale of the vapor exchange is short, ρ_{v10} will generally be near the ice saturation value at T_{10}.

[34] Let us look further at the quantity ρ_{vw}/ρ_{vi}, however. This can be very large and often comparable to $1/\alpha$. We compute the vapor density at temperature T (in °C) as

$$\rho_v(T) = \frac{100\,e\,M_w}{R(T + 273.15)}, \tag{4.2}$$

where M_w (= 18.0160×10^{-3} kg/mol) is the molecular weight of water, R (= 8.31441 J/mol °C) is the universal gas constant, and the 100 provides a vapor density in kilograms per cubic meter when the vapor pressure e is in millibars.

[35] From equations (2.2), (2.3), and (4.2), we see

$$\frac{\rho_{vw}}{\rho_{vi}} = \left(\frac{T_i + 273.15}{T_w + 273.15}\right)\exp\left(\frac{17.966T_w}{T_w + 247.15} - \frac{22.452T_i}{T_i + 272.55}\right) \cdot (1 - 0.000537S), \tag{4.3}$$

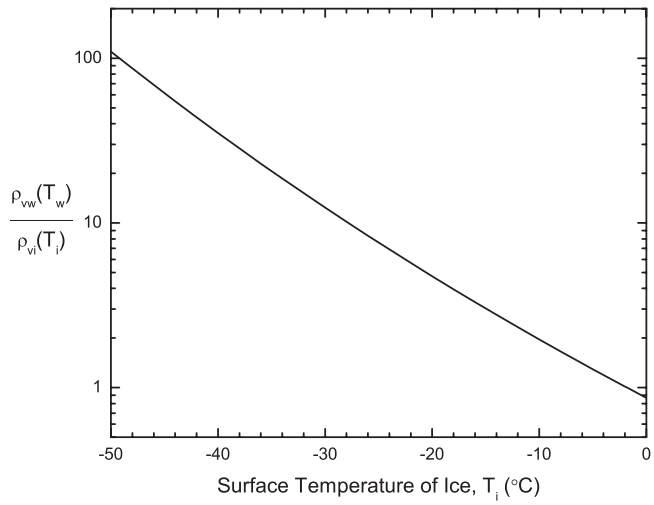

Figure 6. Ratio of saturation water vapor densities figured with respect to saturation over water at temperature T_w ($\rho_{vw}(T_w)$) and over sea ice at temperature T_i ($\rho_{vi}(T_i)$). Here T_w is always −1.8°C, and the salinity of the water is 34 psu.

where, for practical purposes, we have taken

$$\frac{(1.0007 + 3.46 \times 10^{-6}P)6.1121}{(1.0003 + 4.18 \times 10^{-6}P)6.1115} \approx 1. \tag{4.4}$$

The yet unexplained term at the end of equation (4.3) accounts for how salinity S (in psu) depresses the saturation vapor pressure over seawater [e.g., *Roll*, 1965, p. 262].

[36] For most of the year, the temperature of the surface water in leads and polynyas is at its salinity-determined freezing point, about −1.8°C. This is T_w. The ice surface, however, can be much colder. Figure 6 shows ρ_{vw}/ρ_{vi} computed from equation (4.3) as a function of T_i. Clearly, this ratio can be large. For T_i = −10°C, it is 1.96; for −20°C, 4.75; for −30°C, 12.4; and for −40°C, 35.2.

[37] We do not have a definitive estimate for the lead fraction α for any season or Arctic or Antarctic locale, although *Perovich et al.* [2002] report some observations of lead fraction in the vicinity of the SHEBA camp between May and October 1998. The common wisdom is that, in winter, α is between 1 and 5% in the Arctic [e.g., *Gloersen et al.*, 1992]. For T_i = −20°C and α = 5%, from equation (4.1) $\rho_{v10,\mathrm{lim}} = 1.19\rho_{vi}$. Even if α is only 1%, at T_i = −20°C, $\rho_{v10,\mathrm{lim}}$ is still $1.04\rho_{vi}$. For T_i = −30°C, the corresponding values of $\rho_{v10,\mathrm{lim}}$ for α = 5% and α = 1% are $1.57\rho_{vi}$ and $1.11\rho_{vi}$. Table A1 lists these values as well as calculations for other conditions.

[38] Since leads will stay unfrozen longer at higher temperatures, we expect α to be larger at the higher temperatures. For example, when T_i averages −5°C, α is probably no smaller than 5% [*Perovich et al.*, 2002]. Here then, $\rho_{v10,\mathrm{lim}} = 1.02\rho_{vi}$. That is, there is a regulating mechanism in equation (4.1) that tends to keep $\rho_{v10,\mathrm{lim}}$ high. At low temperature, α may be small but ρ_{vw}/ρ_{vi} is large. Conversely, at higher temperatures, α tends to be larger but ρ_{vw}/ρ_{vi} is smaller.

[39] Equations (3.7) and (4.1) also imply that, as the ABL approaches equilibrium, the water vapor that the leads give

up is condensing on the sea ice. That is, eventually, $\rho_{v10} > \rho_{vi}$. With their large-eddy simulation of the plume downwind of a 200-m-wide lead, *Glendening and Burk* [1992] actually saw this transfer of heat from the lead to the downwind ice surface. *Dare and Atkinson* [1999] demonstrated this same turbulent transfer of heat from open water to downwind ice with their numerical model of a 10-km-wide polynya.

[40] Most of our discussion so far has implicitly focused on the winter situation—when the ice is much colder than the open water. But our simple model forecasts relative humidities near ice saturation in the summer, too.

[41] In the height of the Arctic summer during SHEBA (namely, August 1998), all surfaces were wet; and the fraction of open water α was about 18% [*Perovich et al.*, 2002]. That is, the ice surface now had a temperature of 0°C. The water in the leads had also warmed to about 2°C and had freshened to a salinity of about 2 psu (C. A. Paulson, personal communication, 2000). Inserting these values—T_i = 0°C, T_w = 2°C, and S = 2 psu—in equation (4.3), we find that ρ_{vw}/ρ_{vi} = 1.15. Consequently, from equation (4.1) with α = 0.18, the relative humidity with respect to ice saturation seeks a limit of 103% in August.

[42] In essence, the warm leads are now pumping out water vapor even more rapidly than in winter and also cover more area. The ice surface, however, is fixed at 0°C and is, thus, still slow to accept this vapor. As a result, in summer, the ABL still tends to have a relative humidity near ice saturation (which, near 0°C, is also equivalent to water saturation). We see this in Figures 1–3, where the relative humidity with respect to ice is near 100% in the height of summer (say, 15 August 1998, SHEBA day 592).

[43] In summary, because of the leads, there is more than enough water vapor available to keep the ABL saturated with water vapor if the saturation value is computed with respect to ice (which it should be since ice is the dominant water phase in virtually all seasons). And supersaturation becomes more likely with increasing lead fraction and decreasing ice surface temperature [cf. *King and Anderson*, 1999]. Yes, significant supersaturation. Figures 1–4 show occasional relative humidities significantly exceeding 100%. All our instruments showed such episodes, usually simultaneously. With our model suggesting that there is water vapor available to provide such supersaturation, we can no longer doubt such measurements.

[44] After all, to prevent supersaturation, the atmosphere must provide a sink for the excess vapor. The two main sinks for water vapor in the ABL over sea ice are condensation on the surface and condensation as water droplets or ice crystals on cloud condensation or ice nuclei. Our modeling suggests that transfer to the ice surface does not seem rapid enough to entirely relieve the supersaturation. And *Andreas et al.* [1981] demonstrated that, when water vapor from leads is involved, the number of available condensation nuclei can indeed limit the rate at which water vapor is converted to water droplets. Similarly, *King and Anderson* [1999] explained that the limited availability and slow growth of crystals on ice nuclei can allow supersaturation with respect to ice to persist for many hours.

[45] In other words, our casual and formal observations are starting to fit together: the frequent fog, the low clouds, ubiquitous rains of "diamond dust" [*Ohtake et al.*, 1982], all the SHEBA humidity sensors showing relative humidities with respect to ice continually near 100% and often higher, the continual rime and frost forming on all our equipment. Open leads are providing enough water vapor to saturate the polar marine ABL routinely.

4.2. Over the Open Ocean

[46] In contrast, if we set $\alpha = 1$ in equation (3.6), we have the open ocean case:

$$\rho_{v_{10}} = \rho_{vw}[1 - \exp(-t/\tau)]. \tag{4.5}$$

Here ρ_{vw} is the density of water vapor in equilibrium with ocean surface water at temperature T_w, which can, of course, be significantly above −1.8°C.

[47] The relevant timescale in equation (4.5), τ, is still given by equation (3.5); but the values of h, U_{10}, and C_{E10} will be different than for the polar case. For example, the height of the marine boundary layer (MBL) is usually at least 200 m. From measurements during AMTEX (Air Mass Transformation Experiment) in the East China Sea in February 1975, *Wyngaard et al.* [1978] found MBL heights between 680 and 1900 m. Off the California coast in September and October 1976 during CEWCOM (Cooperative Experiment in West Coast Oceanography and Meteorology), *Davidson et al.* [1984] observed MBL heights roughly between 200 and 800 m. If we assume that cloud base corresponds approximately to the height of the MBL, we find in the summary by *White et al.* [1995] of results from five different experiments in various seasons that the height of the MBL is typically between 200 and 1400 m. Finally, our (i.e., P. S. G.) unpublished radiosounding observations over the Labrador Sea in February and March 1997 reiterate that the MBL typically has a mean height well over 1000 m.

[48] Although the value of C_{E10} over the ocean at neutral stability is nearly what it is over leads and polynyas, 1.1–1.2 × 10^{-3} [*DeCosmo et al.*, 1996; *Fairall et al.*, 1996a], the MBL is usually unstably stratified. As a consequence, C_{E10} will be slightly larger than its neutral-stability value [e.g., *Smith*, 1988]. We use $C_{E10} = 1.5 \times 10^{-3}$. Finally, U_{10} can range from 0 to 75 m/s and higher. For demonstration purposes, though, we take it as 5–10 m/s [e.g., *Hsiung*, 1986]. Therefore, we estimate that τ may range from 4 to 40 hours over the open ocean.

[49] Besides the difference in timescales for reaching equilibrium between the polar seas and the open ocean, an equally important consideration is entrainment at the top of the ABL. We do not include entrainment as either a source or a sink in our simple ABL model (equation 3.3). This is probably a fairly accurate assumption for the polar ABL since the prevalent stable stratification would tend to limit exchange across the top of the boundary layer. In fact, if exchange did occur, it would generally moisten the ABL since the temperature is usually higher and the specific humidity is, consequently, also higher above the polar ABL than within it. Over the open ocean, on the other hand, the specific humidity above the MBL is usually lower than within the boundary layer [e.g., *Wyngaard et al.*, 1978], and entrainment at the top of the boundary layer plays an important role in the heat and moisture budgets within the boundary layer [e.g., *Davidson et al.*, 1984]. That is, for the

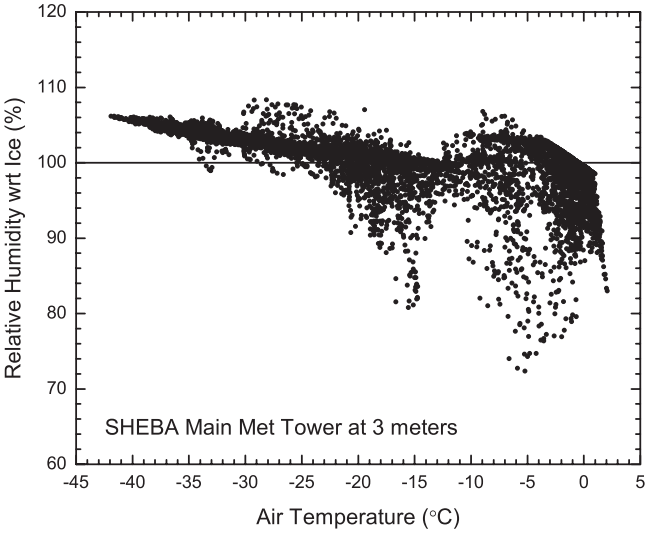

Figure 7. Hourly averaged values of relative humidity with respect to ice plotted versus air temperature, as measured at the 3-m level of the main SHEBA tower.

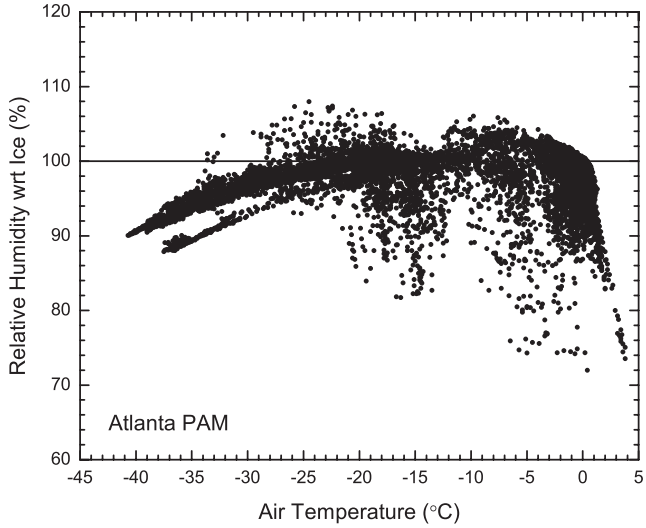

Figure 8. As in Figure 7, except these data came from the PAM station at Atlanta.

MBL, entrainment commonly lowers ρ_{v10} beyond what equation (4.5) would predict.

[50] In summary, polar and marine boundary layers have distinct differences that explain why the former can sustain near-surface relative humidities near saturation while the latter cannot. First, the timescale of the evolution of the ABL over the ocean is longer than it is over polar sea ice, primarily because the boundary layer is deeper. As a result, since the open ocean commonly experiences diurnal forcing that manifests as warming of the sea surface during the day and cooling at night [*Fairall et al.*, 1996b; *Donlon and Robinson*, 1997], ρ_{v10} may not often reach its asymptotic limit. Second, entrainment at its top tends to dry the MBL. Finally, the surface heterogeneity of the ice-covered ocean, even in summer, is also crucial. In winter, the surface temperatures of a sea ice environment can range over 40°C; in summer, they range over a few degrees. Ocean surface temperatures in a given area, in contrast, vary only by tenths of a degree from place to place. Comparing equation (4.5) with equation (3.7) shows that, as a result, the MBL has no way to concentrate the available water vapor as the boundary layer over sea ice does.

5. Instrumental Considerations

[51] Measuring humidity at subzero temperatures is a notorious problem. In fact, *Makkonen* [1996] contends that it is impossible to measure relative humidity accurately at temperatures below 0°C with unheated, solid-state sensors, such as the Vaisala sensors we used at SHEBA. Although we experienced difficulties with our humidity measurements during both SHEBA and ISW, as we will explain, we are not this pessimistic about subzero humidity measurements.

[52] *Anderson* [1994] plotted RH_i versus air temperature measured with a Vaisala HMP35A sensor at Halley Station. The humidity sensor in this HMP35A was a Humicap. His data show a dramatic undersaturation with respect to ice that increases as air temperatures fall farther and farther below −25°C. Figures 7–9 show representative, similar plots of our measurements during SHEBA.

[53] The data from the Vaisala HMD50Y and HMD50U sensors on the PAM stations and on the SPO towers in Figures 8 and 9, respectively, are similar to *Anderson*'s [1994] results. Anderson's instrument, however, used a Humicap to measure humidity, while the PAM and SPO instruments used Intercaps. The curious double tongue at low temperatures in the Atlanta data results, we believe, because several different humidity sensors—obviously with different response characteristics—were switched in and out of that PAM station.

[54] The five Vaisala HMP235 sensors on our main tower, as represented by Figure 7, show the opposite trend at low temperature, however. For these, the measured RH_i values increase progressively above 100% as the temperature falls, in contrast to the behavior that *Anderson* [1994]

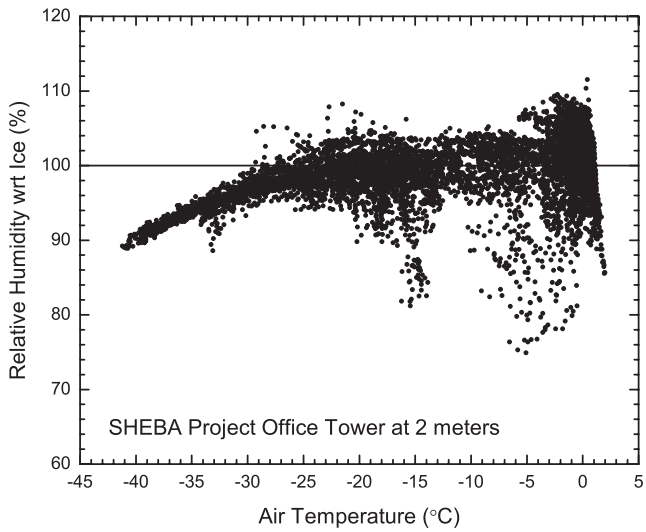

Figure 9. As in Figure 7, except these data came from the 2-m level of the best exposed of the two towers maintained by the SHEBA Project Office.

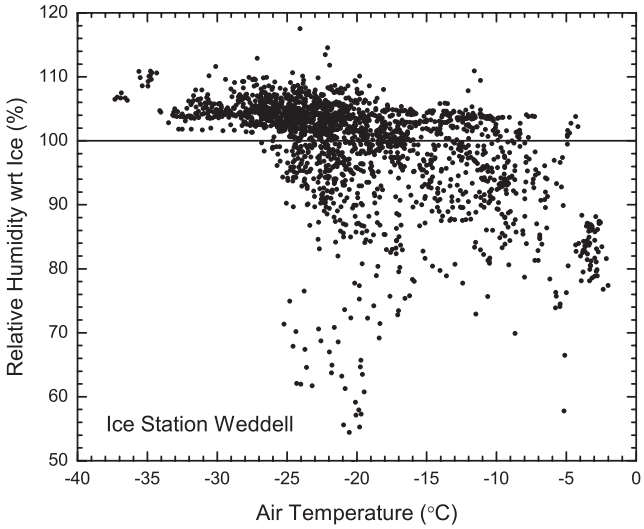

Figure 10. As in Figure 7, except these data came from the cooled-mirror dew-point hygrometer and the platinum resistance thermometer deployed at 5 m on Ice Station Weddell.

saw and that we see in the PAM and SPO sensors. This behavior of the tower instruments is especially curious since those humidity sensors were Humicaps, like Anderson's. We can only speculate that the sensor aspiration or the firmware that computed relative humidity in Anderson's HMP35A was different than for our HMP235's.

[55] Figure 10 shows a similar plot with the four months of measurements we made on ISW with the cooled-mirror dew-point hygrometer and its companion platinum resistance thermometer. The data cloud in this figure has a different behavior than those depicted in Figures 7–9. Although Figure 10 suggests supersaturation with respect to ice at very low temperatures, as does Figure 7, the data do not seem to be nearly as coherent as are the data from the main tower.

[56] Another calibration of two SHEBA Flux-PAM HMD50Y humidity sensors made in the NCAR Sensor Calibration Laboratory expressly for this paper confirmed the behavior of the sensor depicted in Figure 8. These sensors were exposed to a flow at ice saturation for temperatures from 0° to −38.5°C. Both sensors increasingly underestimated the relative humidity with respect to ice saturation by amounts compatible with the values in Figure 8 as the temperature fell from −20° to −38.5°C.

[57] In Table 2, we average the temperature and humidity data presented in Figures 7–10 within 5°C temperature bins. With the exception of the highest two temperature bins for ISW, the tabulated averages agree that, for temperatures above −25°C, the relative humidity with respect to ice is virtually 100%. Since the ISW measurements were in the fall, the only way temperatures there could be in the range −10° to 0°C is under strong warm-air advection from the open ocean to the north.

[58] This ISW observation thus suggests a caveat to our conclusions. In ice-edge regions, under strong on-ice advection, boundary layer air may require transit over several hundred kilometers for the near-surface relative humidity to reach ice saturation. Our one-dimensional model simply does not represent this advective situation; another (advective) timescale comes into play. For example, an air mass moving at 10 m/s takes only about 3 hours to travel 100 km. Since this time is near the small end of the τ range we discussed in section 4, we have little basis to assume that, within a couple hundred kilometers of the ice edge, the near-surface relative humidity is near ice saturation for strong on-ice winds.

[59] A contributing factor to the boundary layer's failure to reach ice saturation is that, for on-ice advection, the surface of the ice in the ice-edge region may not be that much colder than the surface of the open ocean. In fact, during a 150-km transect across the Antarctic marginal ice zone during strong on-ice advection, *Andreas et al.* [1984] measured the ice-surface temperature along the entire transect to be essentially the same as the sea surface temperature just ahead of the ice edge. This situation contrasts with the usual case for leads and polynyas embedded in compact sea ice: In these, the open water is much warmer than the surrounding ice, except in summer.

[60] Figure 9 contains a curious cluster of points between −5° and 0°C that suggests significant supersaturation. SPO personnel noticed these data, thought them suspicious, and thus replaced all their humidity sensors on about SHEBA

Table 2. Averages of Air Temperature (T_a), Relative Humidity With Respect to Ice (RH_i), and the Standard Deviation of RH_i (S.D.) for Various Temperature Ranges From Both SHEBA and Ice Station Weddell[a]

Temp. interval, °C	SHEBA												Ice Station Weddell			
	Main Tower, 3 m				PAM at Atlanta				SPO Tower, 2 m							
	No.	T_a, °C	RH_i, %	S.D., %	No.	T_a, °C	RH_i, %	S.D., %	No.	T_a, °C	RH_i, %	S.D., %	No.	T_a, °C	RH_i, %	S.D., %
[−45,−40]	28	−40.83	105.85	0.22	17	−40.32	90.35	0.17	19	−40.59	89.77	0.68				
(−40,−35]	540	−36.95	104.73	0.59	568	−36.91	91.97	1.91	510	−36.75	92.58	1.06	9	−36.42	107.77	1.65
(−35,−30]	825	−32.84	103.64	0.87	830	−32.67	94.97	2.07	918	−32.69	95.03	1.16	82	−31.86	105.28	2.27
(−30,−25]	636	−27.68	102.75	1.36	745	−27.62	97.77	1.68	796	−27.70	97.76	1.39	330	−26.81	104.34	3.05
(−25,−20]	790	−22.26	101.00	1.84	897	−22.25	99.21	2.28	980	−22.26	99.15	2.11	759	−22.58	100.08	8.39
(−20,−15]	897	−17.61	98.44	3.51	1125	−17.35	98.32	3.48	1178	−17.45	98.83	3.19	404	−17.96	97.18	9.07
(−15,−10]	390	−12.86	98.11	3.54	553	−12.90	98.02	4.20	580	−12.78	98.95	3.72	263	−12.41	97.35	6.76
(−10,−5]	582	−7.30	98.13	5.92	625	−7.23	98.53	5.24	713	−7.33	99.51	4.83	135	−8.23	91.97	8.21
(−5,0]	1940	−1.68	98.10	4.39	1697	−1.75	97.38	4.47	1854	−1.70	100.77	5.20	66	−3.44	85.50	6.69
(0, 5]	828	0.45	96.90	3.18	1011	0.56	95.67	4.48	1021	0.49	102.07	4.79				

[a] The column headed No. shows the number of hourly observations in each temperature interval.

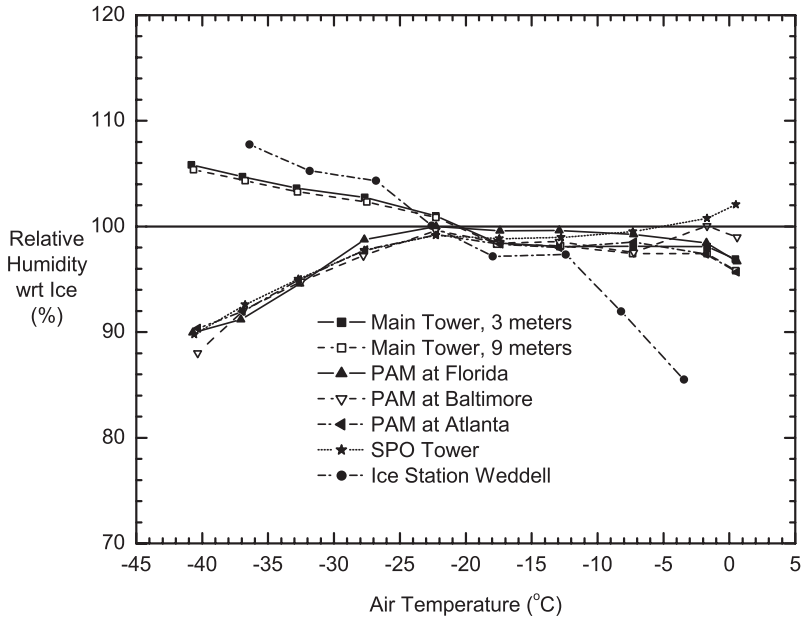

Figure 11. The relative humidity with respect to ice from six SHEBA sensors and one sensor on Ice Station Weddell, averaged in 5°C temperature bins. That bin-averaged relative humidity is plotted versus the bin-averaged temperature for the 5°C temperature bin.

day 610. The step decrease in relative humidity at this time in Figure 3 resulted from this change in sensors. The supersaturations measured by the SPO sensors at temperatures between −5° and 0°C, as shown in Table 2 and in Figure 11, result from this cluster of (presumably) erroneous values. This behavior of the SPO sensors late in the experiment is also consistent with their behavior during the post-experiment calibration. But because these SPO sensors agree well with the PAM sensors earlier in the experiment, when the temperatures were lower, we believe their calibration drifted late in the experiment—probably beginning around SHEBA day 500.

[61] At temperatures below −25°C, Table 2 shows the averages diverging, with the main tower and ISW measurements climbing into supersaturation and the PAM and SPO data falling to significant undersaturation. This divergence explains the difference in monthly averaged humidities between the main tower and the PAM and SPO data for December, January, and February that we pointed out earlier in Table 1.

[62] In Figure 11, we plot the averages from Table 2 and add similar values from the 9-m sensor on our main tower and from the Florida and Baltimore PAM stations, which also had nearly complete SHEBA-long time series. All sensors agree that the average relative humidity with respect to ice is at saturation or is only a few percent below for temperatures between −25° and 0°C.

[63] Below −25°C, however, we have two different observational opinions as to what the relative humidity is. The fact that the ISW dew-point hygrometer predicts supersaturation at temperatures below −25°C, as do the main tower capacitance sensors, could be viewed as decisive. But we have experienced some difficulty in measuring humidity with the General Eastern 1200MPS at low temperatures; it tends to struggle to establish and maintain a frost layer on its mirror and, thus, frequently oscillates around the nominal frost point. *Claffey et al.* [1995] documented some unexplained and unusual behavior in an identical 1200MPS deployed only a few centimeters above the snow surface at ISW. Therefore, although other measurements with a dew-point hygrometer at Halley Station [*King and Anderson*, 1999] showed frequent supersaturations of up to 20%, we are not prepared to say that our measurements showing supersaturation, on average, at temperatures below −25°C are correct.

[64] In fact, *Makkonen* [1996] and *King and Anderson* [1999] argue that an unheated, solid-state sensor, like ours at SHEBA, cannot possibly measure relative humidities above ice saturation at subzero temperatures. The cold sensor simply nucleates ice crystals and, thus, removes the supersaturation.

[65] To resolve the observational discrepancies in Figure 11, we made yet another, more recent, series of calibrations in the NCAR facility using three HMP235 sensors from the ASFG tower and one HMD50Y sensor from the Flux-PAM stations. We performed several series of test during which we exposed the sensors to an airflow at ice saturation (maybe even supersaturation) in temperature steps of about 5°C between +7°C and −48°C. At each new temperature, we gave the calibration chamber between 1 and 3 hours to stabilize before recording the relative humidities that the sensors measured.

[66] These calibration data basically mirror the HMP235 and HMD50Y traces in Figure 11. That is, the HMP235 sensors showed RH_i values above 100% at temperatures below −25°C to −30°C, and the HMD50Y sensor yielded RH_i values that fell increasingly below 100% for temperatures below −25°C.

[67] The one unequivocal conclusion from these tests is that the relative humidity measurements we made at air temperature below −25°C with HMD50Y (on the Flux-PAMs) and HMD50U (on the SPO towers) sensors during SHEBA are biased low—perhaps, by as much as 10% in

relative humidity with respect to ice at −40°C. In light of the averages given in Tables 1 and 2, this result reaffirms our main conclusion that the near-surface relative humidity over sea ice is always near 100% with respect to ice saturation.

[68] Even with these new calibrations, however, we are still unsure how to interpret data from the HMP235 sensors on the ASFG tower. Because the calibration chamber could have been supersaturated, and because the three HMP235 sensors that we calibrated showed supersaturations with respect to ice of 3–6% at −40°C, as do the field data depicted in Figures 7 and 11, we cannot judge whether the HMP235's are biased high or whether supersaturations of 3–6% are, indeed, the norm over sea ice at −40°C.

[69] There are good arguments why supersaturation with respect to ice can exist. For example, during SHEBA, we experienced frequent episodes of liquid-water fog at air temperatures well below 0°C. Since the near-surface air over sea ice is usually close to the temperature of the sea ice, the fog droplets will be also. Suppose that temperature is −15°C. If the fog is to persist, the near-surface vapor pressure must be approximately 1.92 mb (figured with respect to water). The vapor pressure at ice saturation, however, is only 1.66 mb. Thus, in a supercooled fog, the relative humidity can be significantly above ice saturation.

[70] Although our simple ABL model also suggests the increasing likelihood for supersaturation as the temperature falls, we nevertheless prefer to be somewhat conservative. The consensus of the seven sensors represented in Figure 11 is that the near-surface relative humidity with respect to ice is very near 100% and that there is no strong trend with temperature for temperatures between −25° and 0°C. Consequently, we assume—in the face of ambiguous data—that the relative humidity remains near 100% over sea ice for air temperatures down to −45°C.

[71] *Anderson* [1994] used exactly this assumption to apply a linear correction to his humidity data from Halley, which, as we explained, looked like Figures 8 and 9. A true linear correction would be expressed as

$$RH_{i,true} = a\ RH_{i,meas} + b, \tag{5.1}$$

where $RH_{i,meas}$ is the measured relative humidity with respect to ice saturation, and $RH_{i,true}$ is the (presumably true) corrected humidity. To accomplish this correction, Anderson assumed that the highest measured humidity at each temperature corresponded to 100%. That is, he had only one calibration point and, consequently, could evaluate only a or b in equation (5.1), not both. He chose to set the gain a equal to 1 and to evaluate b. In other words, he simply added a constant offset b, determined from the highest $RH_{i,meas}$ at each temperature, to all relative humidities measured at that temperature. An equally justifiable procedure would be to set b = 0 and to evaluate a from the same information. Because of the obvious arbitrariness of either procedure, we prefer to simply assume that the average relative humidity for temperatures below −25°C is at ice saturation.

6. Conclusions

[72] Although the Arctic ABL is "dry" in the sense that it has low absolute humidity by midlatitude standards, its relative humidity is very high—often exceeding saturation with respect to ice. This latter fact is pertinent to matters with which SHEBA is concerned—namely, clouds and fog. We documented this high relative humidity with respect to ice saturation with multiple sensors deployed for a year during SHEBA. Likewise, another long time series from Ice Station Weddell documents the same humidity behavior over Antarctic sea ice. We infer that these two experiments represent typical ABL conditions over perennial sea ice in both the Northern and Southern Hemispheres.

[73] Using a simple time-dependent budget model, we attributed this high relative humidity to the influence of open leads and polynyas. Quite simply, because leads have a relatively warm surface, they give off water vapor much more rapidly than ABL processes can remove it. And we had to assume lead coverage of no more than 5% to see this result. Thus, despite suggestions to the contrary in such venerable sources as *Maykut*'s [1978] study, the polar marine boundary layer is virtually always near saturation with respect to ice.

[74] Two conclusions from our modeling explain why the marine boundary layer, which overlies another saturated surface, is not also routinely near saturation. First, the ocean surface is not as heterogeneous as is perennial sea ice; it does not have embedded within it small areas that are pumping water vapor into the ABL at a rate much faster than the remaining surface can accept it. Second, the timescale for water vapor over sea ice is shorter than the timescale for oceanic water vapor, primarily because the polar ABL is thinner. Synoptic processes are thus not throwing the polar ABL out of equilibrium as often. Also the oceanic timescale is comparable to the diurnal period, while polar sea ice regions rarely experience diurnal forcing.

[75] We do, however, identify persistent shortcomings in our humidity measurements at air temperatures below −25°C. As a result, we do not know whether any of our relative humidity measurements are reliable at these temperatures and are certain that those made with Vaisala HMD50Y and HMD50U sensors are biased low. Because all of our sensors reported virtual saturation with respect to ice for temperatures between −25° and 0°C, however, and because our model likewise implies that ice saturation is easily attainable as temperature falls, we infer that the near-surface relative humidity over sea ice is very near ice saturation down to −45°C.

[76] One obvious use for our result is in estimating the surface vapor flux from polar marine surfaces. Equations (3.1) and (3.2) are the models typically used for this purpose. On the basis of our results, it is now possible to set ρ_{v10} in equations (3.1) and (3.2) without either an in situ or a remote measurement of humidity. Simply compute ρ_{v10} from a measurement of the ice surface temperature T_i or the 10-m air temperature T_{10} and the assumption that the relative humidity is 100% with respect to ice saturation at that temperature.

[77] Likewise, the surface-level vapor pressure is commonly a variable in bulk parameterizations of the incoming longwave radiation in polar regions [e.g., *Launiainen and Cheng*, 1998; *Makshtas et al.*, 1999]. In light of our results, however, it is not necessary to measure humidity to use

Table A1. Values of the Limiting 10-m Absolute Humidity Based on Equation(4.1) (i.e., $\rho_{v10,lim}$) and on Equation (A4) (i.e., $\rho'_{v10,lim}$) for $C_{E10w}/C_{E10i} = 2$[a]

T_i, °C	α, %	$\frac{\rho_v 10,lim}{\rho_{vi}}$	$\frac{\rho'_v 10,lim}{\rho_{vi}}$
−5	5	1.02	1.03
−10	1	1.01	1.02
−10	5	1.05	1.09
−20	1	1.04	1.06
−20	5	1.19	1.36
−30	1	1.11	1.23
−30	5	1.57	2.09

[a] Here also, α is the open water fraction, and T_i is the surface temperature of the sea ice.

these parameterizations. Again, that vapor pressure can simply be estimated from temperature measurements.

Appendix A: If $C_{E10w} \neq C_{E10i}$

[78] Because of the unstable stratification over leads and polynyas but the generally stable stratification over sea ice, C_{E10w} will be larger than C_{E10i}. If we acknowledge this difference, equation (3.3) becomes

$$h\frac{d\rho_{v10}}{dt} = U_{10}[(1-\alpha)C_{E10i}(\rho_{vi} - \rho_{v10}) + \alpha C_{E10w}(\rho_{vw} - \rho_{v10})]. \tag{A1}$$

The solution of this equation, again with $\rho_{v10} = 0$ at $t = 0$, is

$$\rho'_{v10}(t) = \frac{\rho_{vi}\left[1 + \alpha\left(\frac{\rho_{vw}}{\rho_{vi}}\frac{C_{E10w}}{C_{E10i}} - 1\right)\right]}{1 + \alpha\left(\frac{C_{E10w}}{C_{E10i}} - 1\right)}[1 - \exp(-t/\tau')], \tag{A2}$$

where

$$\tau' = \frac{\tau}{1 + \alpha\left(\frac{C_{E10w}}{C_{E10_i}} - 1\right)}. \tag{A3}$$

Because $C_{E10w}/C_{E10i} > 1$, $\tau' < \tau$ and ρ_{v10} in the ABL evolves more rapidly than when $C_{E10w} = C_{E10i}$.

[79] From equation (A2), the asymptotic limit for ρ_{v10} is

$$\rho'_{10,lim} = \frac{\rho_{vi}\left[1 + \alpha\left(\frac{\rho_{vw}}{\rho_{vi}}\frac{C_{E10w}}{C_{E10_i}} - 1\right)\right]}{1 + \alpha\left(\frac{C_{E10w}}{C_{E10_i}} - 1\right)}. \tag{A4}$$

We see that if $C_{E10w}/C_{E10i} = 1$, equation (A4) reduces to our original solution, equation (4.1).

[80] $C_{E10w}/C_{E10i} = 2$ is the largest likely value of this ratio and, thus, provides the biggest difference between the limits represented by equations (4.1) and (A4). We repeat some of the sample calculations in section 4 with this value. Table A1 shows the results.

[81] Although the denominator in equation (A4) is always larger than 1, $\rho'_{v10,lim}/\rho_{vi}$ is a monotonically increasing function of C_{E10w}/C_{E10i}. Consequently, as Table A1 confirms, for $C_{E10w}/C_{E10i} > 1$, $\rho'_{v10,lim} > \rho_{v10,lim}$. In other words, in the more realistic case, when $C_{E10w}/C_{E10i} > 1$, the polar marine ABL would have even higher relative humidity than we described in section 4.

[82] **Acknowledgments.** We thank our colleagues in the Surface Sensing Group of NCAR's Atmospheric Technology Division for supporting our measurements with the Flux-PAM stations. We also thank the many members of our field observing teams; hopefully, you know who you are and realize how much we valued your help. Andy Heiberg, Dean Stewart, and Jumper Bitters of the SHEBA Logistics Team provided unfailing support to us throughout this logistically complex experiment. Finally, we thank Matthew Sturm, Rachel Jordan, Gary Maykut, and two anonymous referees for reviewing the manuscript. The National Science Foundation supported this work with grants to the Army's Cold Regions Research and Engineering Laboratory (OPP-97-02025, OPP-98-14024, and OPP-00-84190), NOAA's Environmental Technology Laboratory (OPP-97-01766 and OPP-00-84323), the Naval Postgraduate School (OPP-97-01390 and OPP-00-84279), and the University of Washington (OPP-97-20144 and OPP-00-84283).

References

Anderson, P. S., Evidence for an Antarctic winter coastal polynya, *Antarct. Sci.*, *5*, 221–226, 1993.
Anderson, P. S., A method for rescaling humidity sensors at temperatures well below freezing, *J. Atmos. Oceanic Technol.*, *11*, 1388–1391, 1994.
Andreas, E. L., A new method of measuring the snow-surface temperature, *Cold Reg. Sci. Technol.*, *12*, 139–156, 1986.
Andreas, E. L., A theory for the scalar roughness and the scalar transfer coefficients over snow and sea ice, *Boundary Layer Meteorol.*, *38*, 159–184, 1987.
Andreas, E. L., Estimating turbulent surface fluxes over polar, marine surfaces, in Preprint volume, Second Conference on Polar Meteorology and Oceanography, 29–31 March 1988, Madison, Wisc., pp. 65–68, Am. Meteorol. Soc., Boston, Mass., 1988.
Andreas, E. L., The atmospheric boundary layer over polar marine surfaces, in *Physics of Ice-Covered Seas*, vol. 2, edited by M. Leppäranta, pp. 715–773, Helsinki Univ. Press, Helsinki, Finland, 1998.
Andreas, E. L., and B. A. Cash, A new formulation for the Bowen ratio over saturated surfaces, *J. Appl. Meteorol.*, *35*, 1279–1289, 1996.
Andreas, E. L., and K. J. Claffey, Air-ice drag coefficients in the western Weddell Sea, 1, Values deduced from profile measurements, *J. Geophys. Res.*, *100*, 4821–4831, 1995.
Andreas, E. L., and A. P. Makshtas, Energy exchange over Antarctic sea ice in the spring, *J. Geophys. Res.*, *90*, 7199–7212, 1985.
Andreas, E. L., and B. Murphy, Bulk transfer coefficients for heat and momentum over leads and polynyas, *J. Phys. Oceanogr.*, *16*, 1875–1883, 1986.
Andreas, E. L., R. M. Williams, and C. A. Paulson, Observations of condensate profiles over Arctic leads with a hot-film anemometer, *Q. J. R. Meteorol. Soc.*, *107*, 437–460, 1981.
Andreas, E. L., W. B. Tucker III, and S. F. Ackley, Atmospheric boundary-layer modification, drag coefficient, and surface heat flux in the Antarctic marginal ice zone, *J. Geophys. Res.*, *89*, 649–661, 1984.
Andreas, E. L., C. W. Fairall, P. S. Guest, and P. O. G. Persson, An overview of the SHEBA atmospheric surface flux program, in Preprint volume, Fifth Conference on Polar Meteorology and Oceanography, 10–15 January 1999, Dallas, Tex., pp. 411–416, Am. Meteorol. Soc., Boston, Mass., 1999.
Andreas, E. L., K. J. Claffey, and A. P. Makshtas, Low-level atmospheric jets and inversions over the western Weddell Sea, *Boundary Layer Meteorol.*, *97*, 459–486, 2000.
Buck, A. L., New equations for computing vapor pressure and enhancement factor, *J. Appl. Meteorol.*, *20*, 1527–1532, 1981.
Claffey, K. J., E. L. Andreas, and A. P. Makshtas, Upper-air data collected on Ice Station Weddell, *Special Rep. 94-25*, 61 pp., U.S. Army Cold Reg. Res. Eng. Lab., Hanover, N. H., 1994. [NTIS: ADA289707.]
Claffey, K. J., E. L. Andreas, A. P. Makshtas, and B. V. Ivanov, In situ measurements of the surface temperature in the western Weddell Sea, in Preprint volume, Fourth Conference on Polar Meteorology and Oceanography, 15–20 January 1995, Dallas, Tex., pp. 86–90, Am. Meteorol. Soc., Boston, Mass., 1995.
Curry, J. A., J. L. Schramm, M. C. Serreze, and E. E. Ebert, Water vapor feedback over the Arctic Ocean, *J. Geophys. Res.*, *100*, 14,223–14,229, 1995.
Dare, R. A., and B. W. Atkinson, Numerical modeling of atmospheric response to polynyas in the Southern Ocean sea ice zone, *J. Geophys. Res.*, *104*, 16,691–16,708, 1999.
Davidson, K. L., C. W. Fairall, P. Jones Boyle, and G. E. Schacher, Ver-

ification of an atmospheric mixed-layer model for a coastal region, *J. Clim. Appl. Meteorol.*, *23*, 617–636, 1984.

DeCosmo, J., K. B. Katsaros, S. D. Smith, R. J. Anderson, W. A. Oost, K. Bumke, and H. Chadwick, Air-sea exchange of water vapor and sensible heat: The Humidity Exchange Over the Sea (HEXOS) results, *J. Geophys. Res.*, *101*, 12,001–12,016, 1996.

Donlon, C. J., and I. S. Robinson, Observations of the oceanic thermal skin in the Atlantic Ocean, *J. Geophys. Res.*, *102*, 18,585–18,606, 1997.

Fairall, C. W., E. F. Bradley, D. P. Rogers, J. B. Edson, and G. S. Young, Bulk parameterization of air-sea fluxes for Tropical Ocean-Global Atmosphere Coupled-Ocean Atmosphere Response Experiment, *J. Geophys. Res.*, *101*, 3747–3764, 1996a.

Fairall, C. W., E. F. Bradley, J. S. Godfrey, G. A. Wick, J. B. Edson, and G. S. Young, Cool-skin and warm-layer effects on sea surface temperature, *J. Geophys. Res.*, *101*, 1295–1308, 1996b.

Glendening, J. W., and S. D. Burk, Turbulent transport from an Arctic lead: A large-eddy simulation, *Boundary Layer Meteorol.*, *59*, 315–339, 1992.

Gloersen, P., W. J. Campbell, D. J. Cavalieri, J. C. Comiso, C. L. Parkinson, and H. J. Zwalley, *Arctic and Antarctic Sea Ice, 1978–1987: Satellite Passive-Microwave Observations and Analysis*, 290 pp., NASA SP-511, Natl. Aeronaut. and Space Admin., Washington, D. C., 1992.

Gow, A. J., D. A. Meese, D. K. Perovich, and W. B. Tucker III, The anatomy of a freezing lead, *J. Geophys. Res.*, *95*, 18,221–18,232, 1990.

Hsiung, J., Mean surface energy fluxes over the global ocean, *J. Geophys. Res.*, *91*, 10,585–10,606, 1986.

ISW Group, Weddell Sea exploration from ice station, *Eos Trans. AGU*, *74*(11), 121–126, 1993.

Kahl, J. D., Characteristics of the low-level temperature inversion along the Alaskan Arctic coast, *Int. J. Climatol.*, *10*, 537–548, 1990.

King, J. C., and P. S. Anderson, A humidity climatology for Halley, Antarctica, based on frost-point hygrometer measurements, *Antarct. Sci.*, *11*, 100–104, 1999.

Launiainen, J., and B. Cheng, Modelling of ice thermodynamics in natural water bodies, *Cold Reg. Sci. Technol.*, *27*, 153–178, 1998.

Lindsay, R. W., Temporal variability of the energy balance of thick Arctic pack ice, *J. Clim.*, *11*, 313–333, 1998.

Mahesh, A., V. P. Walden, and S. G. Warren, Radiosonde temperature measurements in strong inversions: Correction for thermal lag based on an experiment at the South Pole, *J. Atmos. Oceanic Technol.*, *14*, 45–53, 1997.

Mahrt, L., Modelling the depth of the stable boundary-layer, *Boundary Layer Meteorol.*, *21*, 3–19, 1981.

Makkonen, L., Comments on "A method for rescaling humidity sensors at temperatures well below freezing", *J. Atmos. Oceanic Technol.*, *13*, 911–912, 1996.

Makshtas, A. P., *The Heat Budget of Arctic Ice in the Winter*, 77 pp., Int. Glaciol. Soc., Cambridge, England, 1991.

Makshtas, A. P., E. L. Andreas, P. N. Svyashennikov, and V. F. Timachev, Accounting for clouds in sea ice models, *Atmos. Res.*, *52*, 77–113, 1999.

Maykut, G. A., Energy exchange over young sea ice in the central Arctic, *J. Geophys. Res.*, *83*, 3646–3658, 1978.

Militzer, J. M., M. C. Michaelis, S. R. Semmer, K. S. Norris, T. W. Horst, S. P. Oncley, A. C. Delany, and F. V. Brock, Development of the prototype PAM III/Flux-PAM surface meteorological station, in Preprint volume, Ninth Symposium on Meteorological Observations and Instrumentation, 27–31 March 1995, Charlotte, N. C., pp. 490–494, Am. Meteorol. Soc., Boston, Mass., 1995.

Moritz, R. E., and D. K. Perovich (Eds.), SHEBA, a research program on the Surface Heat Budget of the Arctic Ocean: Science plan, *ARCSS/OAII Rep. No. 5*, 60 pp., Polar Sci. Cent., Univ. of Wash., Seattle, 1996.

Moritz, R. E., J. A. Curry, A. S. Thorndike, and N. Understeiner (Eds.), SHEBA, a research program on the Surface Heat Budget of the Arctic Ocean: Prospectus, *ARCSS/OAII Rep. No. 3*, 34 pp., Polar Sci. Cent., Univ. of Wash., Seattle, 1993.

Ohtake, T., K. Jayaweera, and K.-I. Sakurai, Observation of ice crystal formation in lower Arctic atmosphere, *J. Atmos. Sci.*, *39*, 2898–2904, 1982.

Perovich, D. K., et al., Year on ice gives climate insights, *Eos Trans. AGU*, *80*(41), 481–486, 1999.

Perovich, D. K., W. B. Tucker III, and K. A. Ligett, Aerial observations of the evolution of ice surface conditions during summer, *J. Geophys. Res.*, *107*, 10.1029/2000JC000449, 2002.

Persson, P. O. G., C. W. Fairall, E. L. Andreas, P. S. Guest, and D. K. Perovich, Measurements near the Atmospheric Surface Flux Group tower at SHEBA: Near-surface conditions and surface energy budget, *J. Geophys. Res.*, *107*, 10.1029/2000JC000705, 2002.

Roll, H. U., *Physics of the Marine Atmosphere*, 426 pp., Academic, San Diego, Calif., 1965.

Serreze, M. C., J. D. Kahl, and R. C. Schnell, Low-level temperature inversions of the Eurasian Arctic and comparisons with Soviet drifting station data, *J. Clim.*, *5*, 615–629, 1992.

Skony, S. M., J. D. W. Kahl, and N. A. Zaitseva, Differences between radiosonde and dropsonde temperature profiles over the Arctic Ocean, *J. Atmos. Oceanic Technol.*, *11*, 1400–1408, 1994.

Smith, S. D., Coefficients for sea surface wind stress, heat flux, and wind profiles as a function of wind speed and temperature, *J. Geophys. Res.*, *93*, 15,467–15,472, 1988.

Sverdrup, H. U., (Ed.), *The Norwegian North Polar Expedition With the "Maud," 1918–1925, Scientific Results,* vol. II, *Meteorology*, 331 pp., Geofys. Inst., Bergen, Norway, 1933.

Treshnikov, A. F., (Ed.), *Atlas of the Arctic (in Russian)*, 204 pp., Main Off. for Geod. and Cartogr. of the Counc. of Minist. of the USSR, Moscow, 1985.

Vihma, T., Subgrid parameterization of surface heat and momentum fluxes over polar oceans, *J. Geophys. Res.*, *100*, 22,625–22,646, 1995.

Vowinckel, E., and S. Orvig, The climate of the North Polar Basin, in *World Survey of Climatology,* vol. 14, *Climates of the Polar Regions*, edited by S. Orvig, pp. 129–252, Elsevier Sci., New York, 1970.

Walden, V. P., A. Mahesh, and S. G. Warren, Comment on "Recent changes in the North American Arctic boundary layer in winter" by R. S. Bradley et al., *J. Geophys. Res.*, *101*, 7127–7134, 1996.

Wettlaufer, J. S., M. G. Worster, and H. E. Huppert, Solidification of leads: Theory, experiment, and field observations, *J. Geophys. Res.*, *105*, 1123–1134, 2000.

White, A. B., C. W. Fairall, and J. B. Snider, Surface-based remote sensing of marine boundary-layer cloud properties, *J. Atmos. Sci.*, *52*, 2827–2838, 1995.

Wyngaard, J. C., W. T. Pennell, D. H. Lenschow, and M. A. LeMone, The temperature-humidity covariance budget in the convective boundary layer, *J. Atmos. Sci.*, *35*, 47–58, 1978.

Zilitinkevich, S., and D. Mironov, A multi-limit formulation for the equilibrium depth of a stably stratified boundary layer, *Boundary Layer Meteorol.*, *81*, 325–351, 1996.

E. L. Andreas, U.S. Army Cold Regions Research and Engineering Laboratory, 72 Lyme Road, Hanover, NH 03755-1290, USA. (eandreas@crrel.usace.army.mil)

P. S. Guest, Department of Meteorology, Naval Postgraduate School, Monterey, CA 93943-5114, USA. (pguest@nps.navy.mil)

P. O. G. Persson, Cooperative Institute for Research in Environmental Sciences, University of Colorado, Campus Box 216, Boulder, CO 80309, USA. (ola.persson@noaa.gov)

C. W. Fairall, NOAA Environmental Technology Laboratory, 325 Broadway, Boulder, CO 80303-3328, USA. (chris.fairall@noaa.gov)

T. W. Horst and S. R. Semmer, National Center for Atmospheric Research, P.O. Box 3000, Boulder, CO 80307-3000, USA. (horst@ucar.edu; semmer@atd.ucar.edu)

R. E. Moritz, Polar Science Center, University of Washington, 1013 NE 40th Street, Seattle, WA 98105-6698, USA. (dickm@apl.washington.edu)